JOURNAL OF COMPUTATIONAL PHYSICS 112, 138–148 (1994)

A Non-iterative Scheme for Orthogonal Grid Generation with Control Function and Specified Boundary Correspondence on Three Sides

H. J. OH AND I. S. KANG

Department of Chemical Engineering and Advanced Fluids Engineering Research Center, Pohang Institute of Science and Technology, P.O. Box 125, Pohang 790-600, Korea

Received October 15, 1992; revised August 18, 1993

A new numerical scheme is proposed for generating an orthogonal grid in a simply-connected 2D domain. The scheme is based on the idea of decomposition of a global orthogonal transform into consecutive mappings of a conformal mapping and an auxiliary orthogonal mapping, which was suggested by Kang and Leal (*J. Comput. Phys.* **102**, 78 (1992)). The method is non-iterative and flexible in the adjustment of grid spacing. The grid spacing can be controlled mainly by specification of the boundary correspondence up to *three* sides of the boundary. The method is also equipped with a control function that provides further degrees of freedom in the grid spacing adjustment. From a mathematical viewpoint, the proposed scheme can also be regarded as a numerical implementation of the *constructive* proof for the existence of a solution of the orthogonal mapping problem in an arbitrary simply-connected domain under the condition that the boundary correspondence is specified on three sides.

1. INTRODUCTION

The generation of boundary-fitted orthogonal coordinates for a given fixed 2D domain is a long-standing problem of theoretical and practical importance and many methods have been proposed. The most well-known orthogonal mappings are the conformal mappings. Indeed, several efficient methods for numerical construction of conformal mappings have been developed (see the book by Thompson *et al.* [1] and the papers by Fornberg [2] and Symm [3] and the references therein). However, one significant deficiency in the conformal mapping is the non-adjustability of grid spacing. Thus, the methods of orthogonal grid generation have been developed in a way to enlarge the flexibility in adjustment of grid spacing. The numerical scheme proposed in this work is also the result of such an attempt.

In the present work, we are concerned with a *non-iterative* numerical scheme for generating an orthogonal grid in an arbitrary simply-connected 2D domain, the grid points for which are specified at three sides of the domain. All other grid points including the boundary points on the fourth side are determined during the solution process of the mapping problem. The grid generation problem may be represented as shown in Fig. 1, where Ω_x and Ω_ξ denote the physical and computational domains, respectively. Then, the problem we are concerned with can be stated as to find an orthogonal transformation between the points in the computational domain ($(\xi, \eta) \in \Omega_\xi$) and the points in the physical domain ($(x, y) \in \Omega_x$),

$$T_o: (\xi, \eta) \in \Omega_\xi \rightarrow (x, y) \in \Omega_x, \tag{1}$$

under the condition that the correspondence is specified on three sides of the boundary but the other conditions are free.

The numerical scheme proposed in the present work has predecessors. Kang and Leal [4] proposed a *non-iterative* numerical scheme for orthogonal grid generation under the condition that the boundary correspondence is specified on *two* adjacent sides of the boundary. In their method, all other grid points including the boundary points on the two unspecified sides are determined during the process of solution. In order to devise a non-iterative scheme, Kang and Leal proposed the idea of decomposition of a global orthogonal mapping into consecutive mappings of a conformal mapping and an auxiliary orthogonal mapping. Then they incorporated their idea in the so-called covariant Laplace equation method, in which the global mapping is found as the solutions of two covariant Laplace equations. The use of covariant Laplace equations as the grid generating equations was first proposed by Ryskin and Leal [5] as part of their grid generation scheme.

In our numerical scheme, Kang and Leal's method is improved in a way to enlarge the flexibility in adjustmnet of the grid spacing while the advantage of the non-iterative algorithm is maintained. The number of sides, where the boundary correspondence can be specified a priori, is increased to *three* from *two*. As will be shown later, this improvement was made possible by adding an orthogonal

0021-9991/94 $6.00

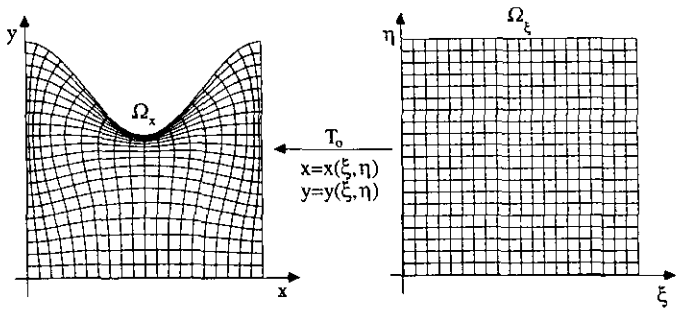

FIG. 1. Orthogonal grid generation in a simply-connected domain with specified boundary correspondence on three sides (Ω_x: the physical domain, Ω_ξ: the computational domain).

grid generation technique for rectangular domains to their method.

Since our scheme is based on Kang and Leal's method, it is very important to understand the covariant Laplace equation method and the idea of the decomposition of orthogonal mapping. Therefore, as preliminaries, the covariant Laplace equation method will be briefly reviewed in Section 2 with discussions on the related grid generation schemes, and the idea of decomposition of orthogonal mapping will be reviewed in Section 3. Then, in Section 4, detailed discussions will be given to the modifications made in this work to improve the numerical scheme of Kang and Leal.

2. COVARIANT LAPLACE EQUATION METHOD

In the covariant Laplace equation method, an orthogonal mapping between the physical (x, y)-domain and the computational (ξ, η)-domain can be found by solving two covariant Laplace equations

$$\frac{\partial}{\partial \xi}\left(f\frac{\partial x}{\partial \xi}\right)+\frac{\partial}{\partial \eta}\left(\frac{1}{f}\frac{\partial x}{\partial \eta}\right)=0, \tag{2a}$$

$$\frac{\partial}{\partial \xi}\left(f\frac{\partial y}{\partial \xi}\right)+\frac{\partial}{\partial \eta}\left(\frac{1}{f}\frac{\partial y}{\partial \eta}\right)=0, \tag{2b}$$

with suitable boundary conditions (see Ryskin and Leal [5]). In (2), f is the distortion function defined by

$$f=\frac{h_\eta}{h_\xi}=\frac{\sqrt{(\partial x/\partial \eta)^2+(\partial y/\partial \eta)^2}}{\sqrt{(\partial x/\partial \xi)^2+(\partial y/\partial \xi)^2}}.$$

However, the problem in the covariant Laplace equation method is that the governing equations are highly nonlinear and consequently very little is known about their general properties. Especially, much work has to be done to answer the following questions (see also the discussions in Kang and Leal [4], and Ryskin and Leal [5]):

(i) What are the suitable boundary conditions that guarantee the existence of a solution?

(ii) If a solution exists, what kind of constraint do we need to obtain a unique solution?

Despite of lack of understanding on the governing equations, the covariant Laplace equation method has been applied in various forms to generate orthogonal grid systems. In their original paper, Ryskin and Leal proposed an ad hoc "weak constraint" method for generating an orthogonal mapping in a given fixed domain. In the weak constraint method, the positions of the grid points are specified on all sides of the boundary but the distortion function, $f(\xi, \eta)$, is adjusted in the course of solution to achieve orthogonality under certain rules (weak constraints). Although several examples are given in their paper, there are two weak points in the method of Ryskin and Leal. First, the existence proof is not available for the mapping problem posed in their method. Second, the solution method is based on the *iterative* adjustment of the distortion function. In view of strong nonlinearities in the governing equations, the convergence of the iterative scheme is not guaranteed. Although there is a report that the convergence of the weak constraint method can be significantly improved by a Bubnov–Galerkin formulation [6], the question of the existence proof and the convergence still remains.

In spite of disadvantages in the form of the weak constraint method, the work of Ryskin and Leal has motivated researchers to seek more successful schemes that are based on the covariant Laplace equation method. Most of schemes developed so far can be classified into one of the following categories according to the grid spacing control:

(i) Class 1. The distortion function $f(\xi, \eta)$ is specified a priori, but the consistent boundary conditions to the specified $f(\xi, \eta)$ are found as part of the solution.

(ii) Class 2. The boundary correspondence is specified on some or all sides of the boundary a priori, but the suitable distortion function $f(\xi, \eta)$ is found as part of the solution.

For the Class 1 methods, the existence of the solution can be proved without difficulty if the distortion function is specified in the product form as $f(\xi, \eta) = \Pi(\xi)\,\Theta(\eta)$ (see Kang and Leal [4]). Among such Class 1 methods, two methods are noteworthy (Duraiswami and Prosperetti [7], and Kang and Leal [4]). Duraiswami and Prosperetti developed a scheme based on the theory of quasi-conformal mapping and the covariant equation method. In their scheme, the conformal module is found first by solving a Laplace equation by the boundary integral technique. Then, with the aid of the module, the covariant Laplace equations

in Eq. (2) are solved subject to the orthogonality condition at the boundary:

$$\frac{\partial x}{\partial \xi}\frac{\partial x}{\partial \eta}+\frac{\partial y}{\partial \xi}\frac{\partial y}{\partial \eta}=0. \tag{3}$$

The governing equations with specified $f(\xi, \eta)$ are linear, but the boundary conditions are still nonlinear. Thus, they proposed an iterative scheme for solving the mapping problem. On the other hand, Kang and Leal [4] proposed a *non-iterative* scheme based on the idea of decomposition of the orthogonal mapping. which will be discussed in the following section. The essence of their method is that, when the distortion function is given in the form $f(\xi, \eta) = \Pi(\xi)\,\Theta(\eta)$, the coupled governing equations in (2) can be transformed into two *uncoupled* linear partial differential equations with Dirichlet boundary conditions.

In the same paper, Kang and Leal proposed also a method in Class 2, which can generate an orthogonal grid system noniteratively when the boundary correspondence is specified at two adjacent sides but the other conditions are free. In fact, their Class 2 scheme is the basis of our new scheme proposed in this paper. Thus, their scheme will be discussed in the following section.

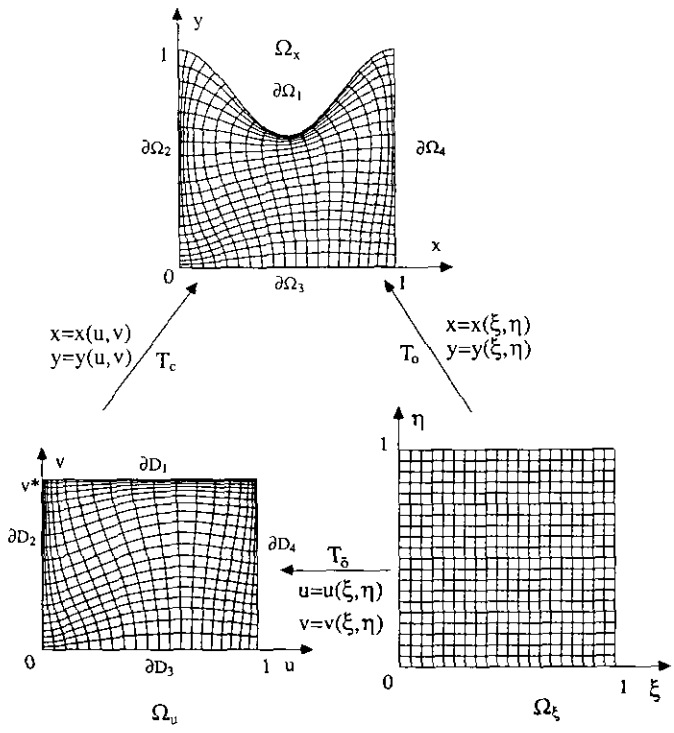

FIG. 2. Decomposition of an orthogonal mapping into a conformal mapping and an auxiliary mapping (Ω_x, the physical domain; Ω_ξ, the computational domain; Ω_u, the auxiliary domain; $\partial\Omega_i$, the ith side of the physical domain; ∂D_i, the ith side of the auxiliary domain).

3. DECOMPOSITION OF ORTHOGONAL TRANSFORM

Kang and Leal [4] suggested that an orthogonal mapping between a given computational domain and a rectangular computational domain (denoted as $T_o: (\xi, \eta) \in \Omega_\xi \to (x, y) \in \Omega_x$) can be decomposed into seqential mappings of a conformal mapping (denoted as $T_c: (u, v) \in \Omega_u \to (x, y) \in \Omega_x$) and an auxiliary orthogonal mapping (denoted as $T_{\tilde{o}}: (\xi, \eta) \in \Omega_\xi \to (u, v) \in \Omega_u$) as shown in Fig. 2. In the figure, Ω_x, Ω_ξ, and Ω_u denote the physical, the computational, and the rectangular auxiliary domains, respectively. The symbols $\partial\Omega_i$ and ∂D_i denote the sides of the physical and auxiliary domains. In Fig. 2, we have scaled the auxiliary and computational domains for convenience. The rectangular auxiliary domain is scaled to have $0 \leqslant u \leqslant 1$ and $0 \leqslant v \leqslant v^*$, where v^* is not free, but it must be determined by the Cauchy–Riemann condition of the conformal mapping, as will be explained later (or see [4]). The computational domain is scaled to have $0 \leqslant \xi \leqslant 1$ and $0 \leqslant \eta \leqslant \eta^*$. Differently from v^*, η^* can be chosen arbitrarily. But in this specific example of a 21×21 grid system, we chose $\eta^* = 1$ for convenience.

The decomposition of orthogonal mapping can be written more formally as

$$T_o = T_c \cdot T_{\tilde{o}}. \tag{4}$$

The key observation in the decomposition is that the distortion function for the global mapping, f, is the same as that for the auxiliary mapping, $\tilde{f}$; i.e.,

$$f(\xi, \eta) = \tilde{f}(\xi, \eta) \qquad \forall (\xi, \eta) \in \Omega_\xi, \tag{5}$$

where $\tilde{f}(\xi, \eta)$ is the ratio of scale factors $\tilde{h}_\eta$ and $\tilde{h}_\xi$ for the auxiliary mapping defined as

$$\tilde{f}(\xi, \eta) = \frac{\tilde{h}_\eta}{\tilde{h}_\xi} = \frac{\sqrt{(\partial u/\partial \eta)^2 + (\partial v/\partial \eta)^2}}{\sqrt{(\partial u/\partial \xi)^2 + (\partial v/\partial \xi)^2}}. \tag{6}$$

The relation (5) follows from the fact that the distortion function for the global mapping is the product of the distortion functions of two sequential mappings ($f = f_c \tilde{f}$) and the distortion function for the conformal mapping is unity ($f_c = 1$).

The significance of the above decomposition is that, given an orthogonal grid in the auxiliary domain (Ω_u), the corresponding orthogonal grid in the physical domain (Ω_x) can be easily generated by using the important relation (5). Thus, a difficult problem of generating an orthogonal grid in the physical domain can be effectively reduced to a simpler problem of generating an orthogonal grid in the rectangular auxiliary domain. (Of course, some conditions imposed in the global mapping problem must be trans-

formed first to the corresponding conditions for the generation of an orthogonal grid in the rectangular auxiliary domain. However, as will be shown later, this transforming process of the given conditions is simple. That is especially the case when the boundary correspondence is specified at some sides.)

Now let us return to the problem of finding the orthogonal grid in the physical domain (Ω_x) which corresponds to a given orthogonal grid in the auxiliary domain (Ω_u). As we can see in Fig. 2, the transform between Ω_x and Ω_u is the conformal mapping. Thus, in principle, we can construct a grid in Ω_x by conformally transforming each grid point in Ω_u to obtain the corresponding point in Ω_x. However, in practice, no simple scheme is available for that purpose. Therefore, we seek a different route. We view the grid system, which we want to find in Ω_x, as the global orthogonal transform of the grid system in the computational domain (i.e., $x_i = x_i(\xi_i, \eta_j)$, $y_j = y_j(\xi_i, \eta_j)$) rather than as the conformal transform of the given grid system in the auxiliary domain (i.e., $x_i = x_i(u_i, v_j)$, $y_j = y_j(u_i, v_j)$). If we take the indirect way, the problem can be solved in a surprisingly simple way. In order to find the global orthogonal mapping, we can use the covariant Laplace equation method. The covariant Laplace equations in (2) can be transformed into two *uncoupled* linear equations with Dirichlet boundary conditions and can be easily solved to produce an orthogonal grid system in the physical domain, if we have

(i) the specified distortion function, $f(\xi, \eta)$, and

(ii) the specified boundary correspondence on all sides of (Ω_x), which is consistent to $f(\xi, \eta)$.

Here we should note that the boundary correspondence cannot be specified arbitrarily but that it must be specified in a consistent way to the given $f(\xi, \eta)$ to guarantee the orthogonality of the resulting grid system. When an orthogonal grid is given in the (u, v)-domain, the above two pieces of information are obtained as follows.

Since we have an orthogonal grid in the (u, v)-domain (i.e., we have an orthogonal transform ($u = u(\xi, \eta)$, $v = v(\xi, \eta)$)), all the derivatives in (6) can be evaluated numerically. Thus, the distortion function for the global mapping at each grid point can be obtained by the formulae (5) and (6). The only thing left is then to find the consistent boundary grid points of the physical domain. As is well known, the conformal mapping ensures the orthogonality of the grid system in the physical domain (except for the non-orthogonally intersecting corner points of the boundary), if the given grid system in the auxiliary domain is orthogonal. Thus, the consistent boundary points that we want to find are only the conformal transformation of the boundary points of the auxiliary domain.

The consistent boundary grid points can be easily obtained by using the boundary integral technique. Since

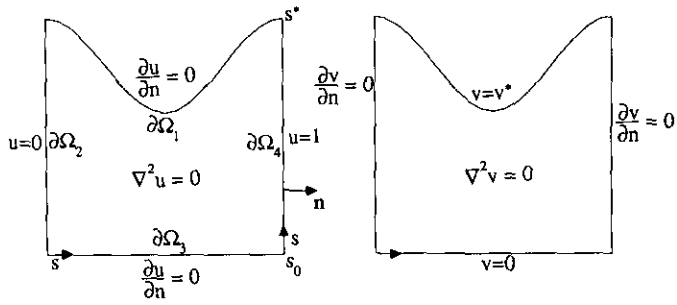

FIG. 3. Two conjugate Laplace equations with boundary conditions for the conformal mapping.

the information that we want to obtain from the conformal mapping part is only the boundary correspondence between Ω_x and Ω_u, it is convenient to consider the inverse mapping T_c^{-1}: $u = u(x, y)$, $v = v(x, y)$, in view of the complicated geometry of the physical domain (see Fig. 2). The inverse mapping T_c^{-1} is also conformal, and governed by two conjugate Laplace equations:

$$\nabla^2 u = \frac{\partial^2 u}{\partial x^2} + \frac{\partial^2 u}{\partial y^2} = 0, \qquad \nabla^2 v = \frac{\partial^2 v}{\partial x^2} + \frac{\partial^2 v}{\partial y^2} = 0. \tag{7}$$

To find T_c^{-1}, we need boundary conditions for the conjugate Laplace equations as shown in Fig. 3, where **n** and s denote the outward unit normal and the arclength along the boundary, starting from a reference point. In the figure, the boundary conditions $u = 0$, $u = 1$, $v = 0$, and $v = v^*$ are due to the scaling we have chosen for the auxiliary domain ($0 \leqslant u \leqslant 1$, $0 \leqslant v \leqslant v^*$), and the conditions $\partial u/\partial n = 0$ and $\partial v/\partial n = 0$ are due to the orthogonality of the conformal coordinates at the boundary. As mentioned earlier, v^* is the maximum value of v and it determines the aspect ratio of the rectangular (u, v)-domain. As explained in Kang and Leal [4], the u-problem can be solved first by using the boundary integral technique and then v^* can be determined from the Cauchy–Riemann condition

$$\frac{\partial u}{\partial n} = \frac{\partial v}{\partial s} \tag{8}$$

along the boundary $\partial\Omega_4$. As we see in the figure, $u(s)$ on $\partial\Omega_1$ and $\partial\Omega_3$, and $(\partial u/\partial n)(s)$ on $\partial\Omega_2$ and $\partial\Omega_4$ are obtained from the boundary integral solution of the u-problem. Thus, v^* can be determined by integrating (8) as

$$v^* = \int_{\partial\Omega_4} \left(\frac{\partial u}{\partial n}\right) ds. \tag{9}$$

Then, the v-problem can be solved similarly to obtain $v(s)$ on $\partial\Omega_2$ and $\partial\Omega_4$.

After two boundary integral solutions are obtained, we have a complete description for u and v as functions of the arclength

$$u = u(s), \qquad v = v(s). \tag{10}$$

Here, we should note that one of $u(s)$ and $v(s)$ is a monotonic function (the other is constant) and its inverse exists on each side of the boundary. The information in (10) can be used to obtain the boundary correspondence between the physical domain and the auxiliary domain. Let us first consider a given point on the boundary of the physical domain. Then the arclength to the point, s, is determined to compute $u(s)$ and $v(s)$ values. The obtained values (u, v) define the corresponding boundary point of the auxiliary domain. Conversely, if a boundary point is given at a certain side of the auxiliary domain (i.e., (u, v) is given), then one of two functions in (10) is a monotonic function on the corresponding side of the physical domain. Thus, the arclength s to the corresponding point of physical domain is obtained by inverting the monotonic function. Since the (x, y)-coordinate of the boundary point can be represented as $x = x(s)$ and $y = y(s)$, the x and y values for the the corresponding boundary point are determined.

Kang and Leal applied the above idea of decomposition to generate an orthogonal grid in a 2D domain when the boundary correspondence is specified on *two adjacent* sides of the boundary as shown in Fig. 4. In Fig. 4, the boundary correspondence is specified at the sides $\partial\Omega_2$ and $\partial\Omega_3$. The method of Kang and Leal can be summarized as:

(i) By using the information from the boundary integral solution, the grid points on the two corresponding adjacent sides of the auxiliary (u, v)-domain (i.e., ∂D_2 and ∂D_3) are determined.

(ii) An orthogonal grid is generated in the auxiliary (u, v)-domain under the assumption that the corresponding points on the opposite sides have the same u- or v-values. Under this assumption, the grid system is simply a non-uniform rectangular grid as shown in Fig. 4. In this case, the orthogonal transform between (u, v)-domain and (ξ, η)-domain can be represented by $u = u(\xi) = u_b(\xi)$ and $v = v(\eta) = v_b(\eta)$, where $u_b(\xi)$ and $v_b(\eta)$ denote the specified boundary correspondences on ∂D_3 and ∂D_2 that are obtained in the step (i).

(iii) By using the formulae (5) and (6), the distortion function for the global mapping, $f(\xi, \eta)$ is computed for all grid points.

(iv) The boundary grid points on $\partial\Omega_1$ and $\partial\Omega_4$ of the physical domain corresponding to the sides ∂D_1 and ∂D_4 of the auxiliary domain are determined by using the information from the boundary integral computation.

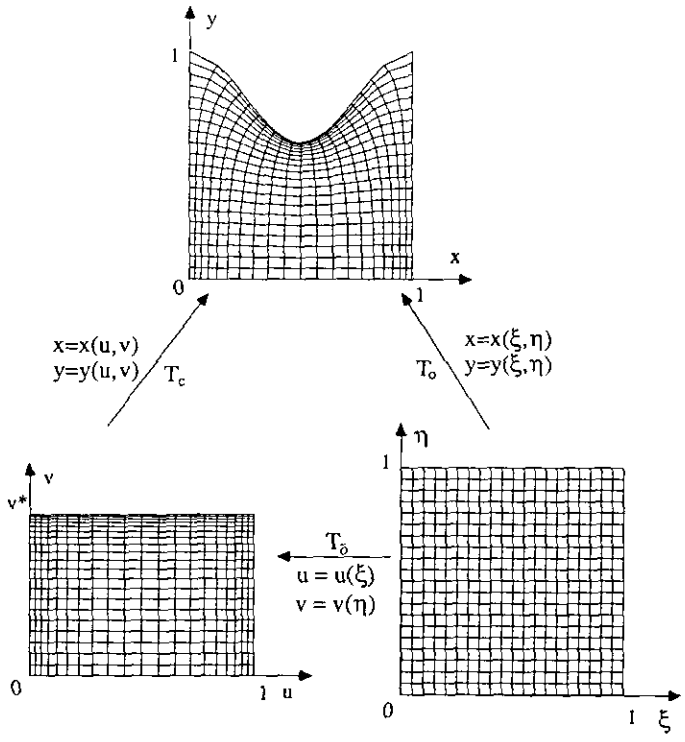

FIG. 4. The idea of decomposition of orthogonal mapping as was used in Kang and Leal [4] (only the simple orthogonal grid generation $u = u(\xi)$, $v = v(\eta)$ was considered for the auxiliary domain).

(v) The covariant Laplace equations in (2) with specified $f(\xi, \eta)$ are solved with the Dirichlet type boundary conditions.

Thus far, we have discussed the method of Kang and Leal. As mentioned earlier, our new scheme is also based on the idea of decomposition of orthogonal transform, and it can be considered as an improved version of their scheme. In the following section, a detailed discussion will be given to what is added in our scheme to improve Kang and Leal's method.

4. ORTHOGONAL GRID GENERATION IN A RECTANGULAR AUXILIARY DOMAIN

As discussed in the preceding section, the global mapping problem can be effectively reduced to the problem of orthogonal grid generation in a rectangular auxiliary domain. Thus, the most important step in our method should be the generation of an orthogonal grid in a rectangular (u, v)-domain under the condition that the boundary correspondence is specified on three sides. We are now concerned with this subproblem.

Let us consider the global mapping problem and see again the physical domain in Fig. 2. The grid system in Fig. 2 was prepared with the specified boundary correspondence on three sides, $\partial\Omega_1$, $\partial\Omega_2$, and $\partial\Omega_3$. The first step

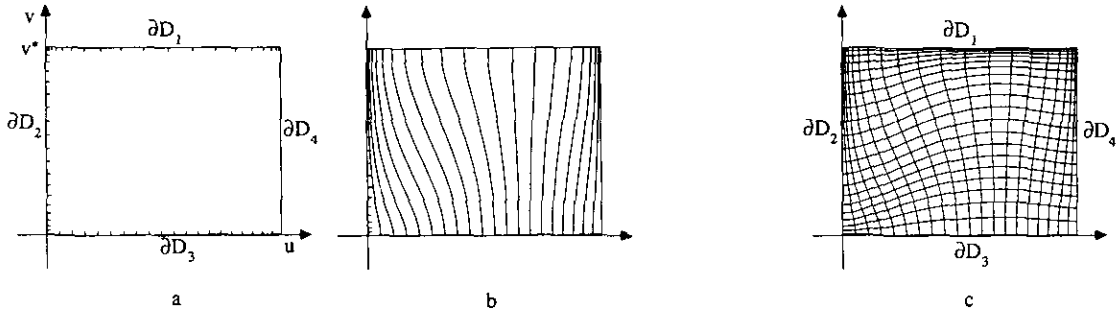

FIG. 5. The procedures for generating an orthogonal grid in a rectangular domain: (a) The specified boundary correspondence on three sides is obtained from the given boundary correspondence for the physical domain; (b) The boundary points on ∂D_1 and ∂D_3 are connected according to (11); (c) The $\eta = \text{const}$ lines are found.

in our scheme starts with finding the boundary points on the corresponding sides of the rectangular auxiliary domain (i.e., ∂D_1, ∂D_2, and ∂D_3) by using the information from the boundary integral solution. After this step, for the auxiliary (u, v)-domain, we have the specified boundary correspondence on three sides as shown in Fig. 5a. Now, we want to generate an orthogonal grid in the rectangular auxiliary domain according to the procedures shown below.

First, we connect the grid points on ∂D_1 and ∂D_3 smoothly and orthogonally at the boundaries. To do that we assume that we have continuous functional relationships $\xi = p_1(u)$ on ∂D_1 and $\xi = p_3(u)$ on ∂D_3, even though we have discrete information on the functional relationships. Then we assume that ξ value at the internal points of (u, v)-domain can be represented as

$$\xi = p_3(u) + [p_1(u) - p_3(u)]\, q(v), \tag{11}$$

where $q(v)$ is a monotonically increasing function that satisfies the four conditions

$$q(0) = 0, \quad q(v^*) = 1, \quad q'(0) = 0, \quad q'(v^*) = 0. \tag{12}$$

The last two conditions are from the orthogonality condition $\partial\xi/\partial v = 0$ at ∂D_1 and ∂D_3. In fact, infinitely many monotonic functions for $q(v)$ can satisfy the four conditions. As will be shown later, this fact provides a considerable degree of freedom in the grid spacing adjustment; i.e., $q(v)$ can be used as a control function. Several reasonable candidates for the control function include

$$q(v) = 3\left(\frac{v}{v^*}\right)^2 - 2\left(\frac{v}{v^*}\right)^3 + a\left(\frac{v}{v^*}\right)^2\left(\frac{v}{v^*} - 1\right)^2 \tag{13}$$

and

$$q(v) = \frac{1}{2}\left[1 + \sin\left(\frac{v}{v^*}\pi - \frac{\pi}{2}\right)\right] + a\left[1 - \cos 2\left(\frac{v}{v^*}\right)\pi\right], \tag{14}$$

where a can be considered as a control parameter for the adjustment of grid spacing and the range of a is limited by the condition of monotonic function.

Now the functions $p_1(u)$ and $p_3(u)$ are constructed as piecewise smooth functions by using the discrete information given on the sides ∂D_1 and ∂D_3 as

$$p_1(u) = \left(\frac{u_{i+1}^{(1)} - u}{u_{i+1}^{(1)} - u_i^{(1)}}\right)\xi_i + \left(\frac{u - u_i^{(1)}}{u_{i+1}^{(1)} - u_i^{(1)}}\right)\xi_{i+1} \tag{15}$$

for $u_i^{(1)} \leqslant u \leqslant u_{i+1}^{(1)}$ on ∂D_1, and

$$p_3(u) = \left(\frac{u_{i+1}^{(3)} - u}{u_{i+1}^{(3)} - u_i^{(3)}}\right)\xi_i + \left(\frac{u - u_i^{(3)}}{u_{i+1}^{(3)} - u_i^{(3)}}\right)\xi_{i+1} \tag{16}$$

for $u_i^{(3)} \leqslant u \leqslant u_{i+1}^{(3)}$ on ∂D_3, where $u_i^{(1)}$ (or $u_i^{(3)}$) denotes the u-value of the boundary grid point at $\xi = \xi_i$ on ∂D_1 (or ∂D_3). The accuracy of the approximation may be improved, but here we adopt the above simple representation for convenience.

After this step, we have the coordinate lines in (u, v)-domain corresponding to $\xi = \xi_i$, $i = 1, 2, \ldots, n$, as shown in Fig. 5b. (In principle, we can find those lines by inverting the functional relationship (11) for given ξ and v. However, we do not have to generate the coordinte lines explicitly. In fact, the internal grid points are determined by the procedure that will be explained later. Nevertheless, for the moment, we assume that we have those grid lines for better understanding). Now, we want to generate $\eta = \text{const}$ coordinate lines. This goal can be easily achieved by using the fact that the unit tangent to the line of $\eta = \text{const}$ coincides with the unit normal to the $\xi = \text{const}$ line at the grid point.

Let l be the arclength along the $\eta = \text{const}$ line measured from the grid point on ∂D_2. Then the orthogonality imposes relations

$$\frac{du}{dl} = \frac{\partial\xi/\partial u}{\sqrt{(\partial\xi/\partial u)^2 + (\partial\xi/\partial v)^2}}, \qquad \frac{dv}{dl} = \frac{\partial\xi/\partial v}{\sqrt{(\partial\xi/\partial u)^2 + (\partial\xi/\partial v)^2}}. \tag{17}$$

As we have seen in (11), ξ is given as a function of u and v. Thus du/dl and dv/dl are also functions of u and v; i.e., they are given for each $\eta = \eta_j$ line in the forms as

$$\frac{du}{dl} = f_1(u, v), \qquad \frac{dv}{dl} = f_2(u, v) \tag{18a), (18b)}$$
$$u = 0 \text{ at } l = 0 \qquad v = v_j^{(2)} \text{ at } l = 0,$$

where $v_j^{(2)}$ is the v value of the grid point at ∂D_2 corresponding to the $\eta = \eta_j$ line. Now, the system of ordinary differential equations (18) can be integrated numerically. In the course of integration, the ξ value is evaluated by (11) and is compared with the ξ_i values. Since ξ is a monotonically increasing function of l, we can easily find the u and v values for the grid point corresponding to (ξ_i, η_j). Then, we assign the u and v values as (u_i, v_j) for the grid point corresponding to (ξ_i, η_j). In this way, we generate an orthogonal grid system in a rectangular domain as shown in Fig. 5c.

Now we compute the distortion function $\tilde{f}(\xi, \eta)$ at each grid point of the (u, v)-domain. Since we have $(u_i(\xi_i, \eta_j), v_j(\xi_i, \eta_j))$ for all grid points, $\tilde{f}(\xi_i, \eta_j)$ can be numerically evaluated at each point by the formula

$$\tilde{f}(\xi_i, \eta_j) = \left.\frac{\tilde{h}_\eta}{\tilde{h}_\xi}\right|_{(i,j)} \tag{19}$$

where

$$\tilde{h}_\eta = \sqrt{(\partial u/\partial \eta)^2 + (\partial v/\partial \eta)^2},$$
$$\tilde{h}_\xi = \sqrt{(\partial u/\partial \xi)^2 + (\partial v/\partial \xi)^2}.$$

Then we assign $\tilde{f}(\xi_i, \eta_j)$ to $f(\xi_i, \eta_j)$ for the distortion function for the global mapping according to Eq. (5). During the course of finding the $\eta = \eta_j$ lines in the (u, v)-domain, we also find the boundary grid points on ∂D_4. We again transform this boundary information on ∂D_4 to find the boundary grid points on $\partial \Omega_4$ of the physical domain by using the boundary integral solution shown in Section 3.

Now, we are equipped with all the necessary information for the governing covariant Laplace equations in (2), i.e., the Dirichlet type boundary conditions and the distortion function $f(\xi, \eta)$. Here we should note that the boundary points of the physical domain (the specified points on $\partial \Omega_1$, $\partial \Omega_2$, $\partial \Omega_3$, plus the obtained points on $\partial \Omega_4$) form the consistent boundary correspondence to the obtained $f(\xi, \eta)$ because the grid is orthogonal at all the conformally corresponding points of the auxiliary domain. As mentioned earlier, the equations are *uncoupled* and linear and can be solved very easily to find an orthogonal grid in the physical domain.

Before presenting several examples of the orthogonal grid systems generated by the new scheme, we want to show that the Class 2 scheme of Kang and Leal is a special case of our more general scheme. The specification of boundary correspondence on two adjacent sides ($\partial \Omega_2$ and $\partial \Omega_3$) as shown in Fig. 4 is equivalent to the specification of boundary correspondence on ∂D_2 and ∂D_3 of the auxiliary domain. The extra constraint in their scheme that the corresponding points of the opposite sides have the same u- or v-values (see step (ii) of their scheme in Section 3) is equivalent to taking the assumption that $p_1(u) = p_3(u)$ in our method. As we can see in (11), if $p_1(u) = p_3(u)$, then $\xi = \text{const}$ lines are straight and consequently $\eta = \text{const}$ lines also become straight. Thus we have the non-uniform rectangular grid system in (u, v)-domain as shown in Fig. 4. Therefore, in addition to arbitrary specification on ∂D_2 and ∂D_3, if we specify the boundary correspondence at $\partial \Omega_1$ in a way to satisfy the constraint $p_1(u) = p_3(u)$, then our scheme reduces to the scheme of Kang and Leal.

5. EXAMPLES OF APPLICATIONS

5.1. *Numerical Specifications*

We have applied the proposed scheme to generate several orthogonal grid systems. The detailed characteristics of the generated grid systems will be discussed in the following subsections. In this subsection, we limit our discussion to more general information that has been adopted in all the sample grid generation problems.

In our numerical scheme, we need three different kinds of basic numerical tools:

(i) The boundary integral technique for solving the conjugate Laplace equations in (7).

(ii) The numerical integrator for the ordinary differential equations in (17).

(iii) The linear PDE solver for the covariant Laplace equations in (2) with Dirichlet boundary conditions.

For the part of boundary integral computation, we specified the nodal points of the boundary elements in a way that the nodal points coincide with the boundary grid points on three specified sides of the boundary. For the unspecified fourth side, the nodal points were taken based on the equidistance element. For an $(N_\xi + 1) \times (N_\eta + 1)$ grid system, the total number of nodal points was $2 \times (N_\xi + N_\eta)$. The above choice was made mainly for convenience. In fact, the number and positions of nodal points may be chosen independently of the specified boundary grid points.

For the integration of ordinary differential equations in (17), we have used the fourth-order Runge–Kutta method with the step size of integration $\Delta l = 10^{-3}$ (we have tested several cases with a finer step size $\Delta l = 10^{-4}$, but the results were almost identical).

The covariant Laplace equations in (2) with specified $f(\xi, \eta)$ and Dirichlet boundary conditions can be trans-

formed to two *uncoupled* systems of linear algebraic equations after discretization (one for x-coordinates and the other for y-coordinates). For an $(N_\xi+1)\times(N_\eta+1)$ grid system, each system of linear algebraic equations has $(N_\xi-1)\times(N_\eta-1)$ unknowns. In the present study, we have used the ADI method to solve the systems of linear algebraic equations. The convergence check for this ADI step was made by the criterion

$$|\text{maximum residual}| < 10^{-5}.$$

We have also checked the convergence with more stringent criterion of 10^{-7} in several cases, but we could not find any considerable change in solutions.

The orthogonality of each generated grid system was tested in the same way as in Chikliwala and Yortsos [8] and Allievi and Calisal [6]. At all grid points, the angle was evaluated according to

$$\cos\theta = \frac{x_\xi x_\eta + y_\xi y_\eta}{(x_\xi^2+y_\xi^2)^{1/2}(x_\xi^2+y_\eta^2)^{1/2}}. \tag{20}$$

As the measures for the degree of deviation from orthogonality, two indices MDO and ADO were adopted, where MDO represents the maximum deviation from orthogonality and is defined by

$$\text{MDO} = \max_{i,j}\left|\frac{\pi}{2}-\theta_{ij}\right|, \tag{21}$$

and ADO represents the average deviation and is defined by

$$\text{ADO} = \frac{1}{(N_\xi+1)(N_\eta+1)}\sum_{i,j}\left|\frac{\pi}{2}-\theta_{ij}\right|, \tag{22}$$

for an $(N_\xi+1)\times(N_\eta+1)$ grid system.

In the following subsections, several grid systems generated by our new scheme will be presented. All computation for grid generation was made with double precision on the workstation MIPS CR3240.

5.2. *Orthogonal Grid Generation in an Asymmetric Wavy Region*

As a first example, we considered orthogonal grid generation in an asymmetric wavy region as shown in Fig. 6. The same geometry was considered also by previous investigators [6, 8]. As in Chiliwala and Yortsos [8], the right side of the boundary (corresponding to $\xi=1$) is defined by

$$x = 0.75 + H\cos(\pi y), \qquad 0 \leqslant y \leqslant 1. \tag{23}$$

To generate grid systems, we specified the boundary correspondence on the top ($y=1$ corresponding to $\eta=1$), bottom ($y=0$ corresponding to $\eta=0$), and left ($x=0$ corresponding to $\xi=0$) sides. For the top and bottom sides, the boundary grid points were specified based on the equidistance distribution. For the left side, we considered the following two cases:

(i) Equidistance correspondence, i.e., $y=\eta$.

(ii) Downward shifted correspondence according to $y = 1-[0.2(1-\eta)+0.8\sin(\pi/2)(1-\eta)]$.

For the control function $q(v)$, which is defined in (11), we used

$$q(v) = 3\left(\frac{v}{v^*}\right)^2 - 2\left(\frac{v}{v^*}\right)^3. \tag{24}$$

In Fig. 6, the grid systems generated with the shifted boundary correspondence are shown for the H values 0.25, 0.35, and 0.45. The orthogonality characteristics of the grid systems will be discussed later. (For the cases of equidistance correspondence on the left side, only the orthogonality characterists will be given later.)

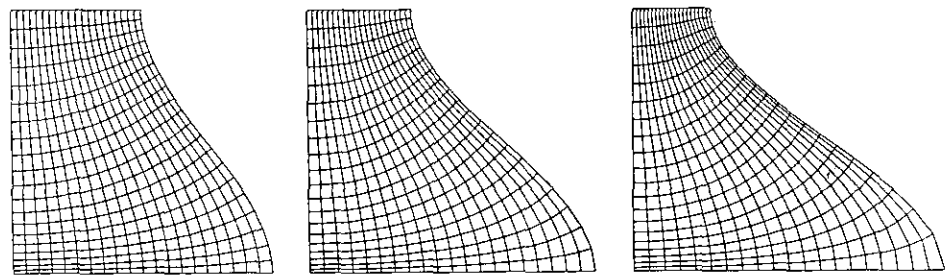

a b c

FIG. 6. Orthogonal grid systems generated in asymmetric regions (top side ($y=1$); bottom side ($y=0$); left side ($x=0$); right side ($x=0.75+H\cos(\pi y)$)): (a) $H=0.25$; (b) $H=0.35$; (c) $H=0.45$. The boundary correspondence was specified on the top, bottom, and left sides (top and bottom sides, equidistance; left side, $y=1-[0.2(1-\eta)+0.8\sin(\pi/2)(1-\eta)]$).

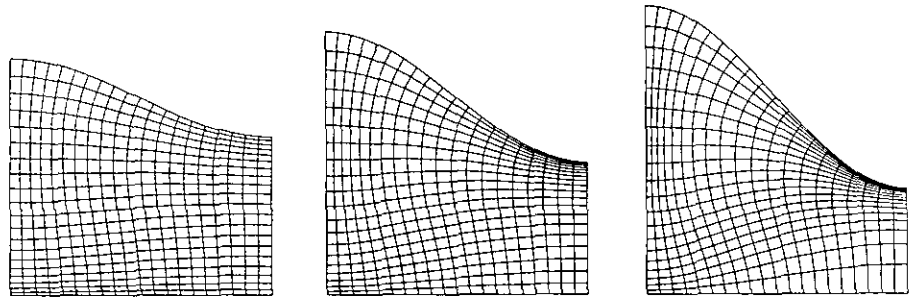

FIG. 7. Orthogonal grid systems generated in asymmetric regions (top side ($y = 0.75 + H\cos(\pi x)$); bottom side ($y = 0$); left side ($x = 0$); right side ($x = 1$)): (a) $H = 0.15$; (b) $H = 0.25$; (c) $H = 0.35$. The boundary correspondence was specified on the top, bottom, and left sides (top side, $x = \xi$; bottom side, equidistance; left side, $y = (0.75 + H)[1 - \{0.2(1 - \eta) + 0.8\sin(\pi/2)(1 - \eta)\}]$).

In our scheme we can specify the boundary correspondence up to three sides. In order to generate orthogonal grid systems with different choices of the specified sides, we considered the geometry as shown in Fig. 7. The geometry was considered only for convenience in the specification of the boundary correspondence and in fact is the same as that considered in Fig. 6. As in other examples, the boundary correspondence is specified on the top, bottom, and left sides. The boundary grid points on the top side were specified according to ($x = \xi$, $y = 0.75 + H\cos(\pi\xi)$) and at the bottom side according to the equidistance correspondence. For the left side, we considered also the two cases of boundary correspondence: the equidistance correspondence and the downward shifted correspondence as for the cases in Fig. 6. In Fig. 7, the grid systems generated with the shifted boundary correspondence are shown for $H = 0.15$, 0.25, and 0.35. As we can see in Fig. 7c, the crowding phenomenon near the upper right corner becomes serious as H increases (see Menikoff and Zemach [9] for a detailed discussion on the crowding phenomenon). When the equidistance boundary correspondence was adopted for the left side, the crowding phenomenon was more serious and successful grid systems could not be obtained for the cases $H \geqslant 0.35$.

TABLE I

Orthogonality Characteristics of the 21 × 21 Grid Systems

		MDO–ADO (degrees)			
Geometry	Correspondence	$H = 0.15$	$H = 0.25$	$H = 0.35$	$H = 0.45$
Fig. 6	Shifted[a]	2.2–0.3	2.1–0.6	3.9–1.0	5.7–1.8
Fig. 6	Equal[b]	2.6–0.2	3.1–0.2	6.5–0.3	15.0–0.5
Fig. 7	Shifted	3.8–1.7	2.7–1.4	2.9–0.5	—
Fig. 7	Equal	2.6–1.3	4.5–0.6	—	—

[a] Downward shifted correspondence on the left side.
[b] Equidistance correspondence on the left side.

TABLE II

Effects of Mesh Size on the Orthogonality Characteristics

	MDO–ADO (degrees)				
Case	6 × 6	11 × 11	16 × 16	21 × 21	31 × 31
Fig. 6a ($H = 0.25$)	6.7–1.0	2.8–0.7	2.3–0.6	2.1–0.6	2.1–0.5
Fig. 6b ($H = 0.35$)	10.0–1.3	5.3–1.1	3.8–1.1	3.9–1.0	3.4–1.0
Fig. 6c ($H = 0.45$)	13.5–2.6	7.4–1.9	6.2–1.8	5.7–1.8	5.8–1.8
Fig. 7b ($H = 0.25$)	7.0–1.9	2.5–1.2	2.6–1.3	2.7–1.4	2.8–1.4

The orthogonality characteristics in terms of MDO and ADO are given in Table I for the 21 × 21 grid systems considered in Figs. 6 and 7 (both cases of the equidistance and shifted specification on the left side). As we can see in Table I, the orthogonality characteristics are generally good for the grid systems in Fig. 6. As we can see in Fig. 6, the grid system becomes coarser near the lower right corner as H increases. Although the grid systems for the cases of equidistance specification at the left side are not given, we may easily expect that the resulting grid systems become even coarser near the lower right corner. Due to that effect, the MDO values are larger for the cases of equidistance specification than for the cases of shifted correspondence.

The effects of mesh size on the orthogonality characteristics were also tested for the cases considered in Figs. 6a–c and 7b. The results of MDO and ADO for each case are shown in Table II. As we can see in the table, the

TABLE III

Effects of Mesh Size on the Computation Time

	CPU time (seconds)				
Case	6 × 6	11 × 11	16 × 16	21 × 21	31 × 31
Fig. 6a ($H = 0.25$)	1.6	6	13	24	55
Fig. 6c ($H = 0.45$)	1.6	6	13	23	52

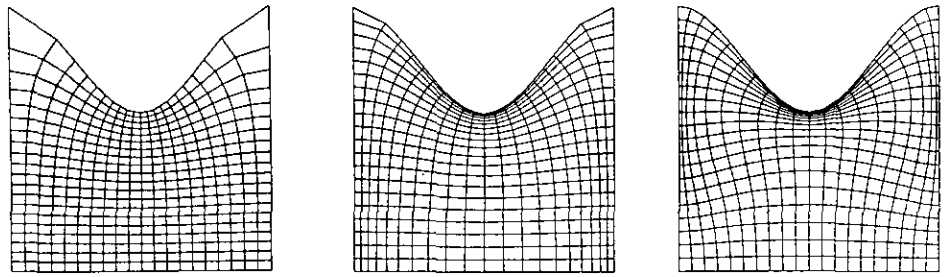

FIG. 8. Orthogonal grid systems generated in a symmetric region (top side ($y = 0.8 + 0.2\cos(2\pi x)$); bottom side ($y = 0$); left side ($x = 0$); right side ($x = 1$)): (a) specified $f = v^*$; (b) specified boundary correspondence on two sides (left side, equidistance; bottom side, $x = \xi - 0.08\sin(2\pi\xi)$); (c) specified boundary correspondence on three sides (top side ($x = \xi$); left and bottom sides, equidistance) with the control function $q(v) = 3(v/v^*)^2 - 2(v/v^*)^3$.

orthogonality characteristics are not very sensitive to the mesh size if the grid is finer than the 16×16 grid.

Typical computation times are listed in Table III as functions of the mesh size for the cases considered in Figs. 6a ($H = 0.25$) and 6c ($H = 0.45$). In these examples, the computation time is not sensitive to the geometry change but it is a function of the number of grid points. The results show that the computation time is approximately proportional to the total number of grid points.

Thus far, we have seen how the orthogonality characteristics of a grid system depend on the factors such as the geometry, the way of specification of boundary correspondence, and the mesh size. In the following subsection, further examples will be discussed with particular emphasis on the effect of control function.

5.3. *Orthogonal Grid Systems in a Symmetric Wavy Region*

In this subsection, we consider orthogonal grid generation in a wavy region as shown in Fig. 8. Similar geometry has been considered also by previous investigators [5, 6, 8, 10, 11]. The top side of the boundary ($\partial\Omega_1$) is given by

$$y = 0.8 + 0.2\cos(2\pi x), \qquad 0 \leqslant x \leqslant 1.$$

For the control function $q(v)$, we used again

$$q(v) = 3\left(\frac{v}{v^*}\right)^2 - 2\left(\frac{v}{v^*}\right)^3. \tag{25}$$

In Fig. 8, one example (c) obtained by the present method is shown with the orthogonal grid systems (a and b) obtained by the method of Kang and Leal [4]. The grid system (a) was obtained by using the specified distortion function $f(\xi, \eta) = v^*$, and (b) was obtained by specifying the boundary correspondence on two sides as ($x = 0$, $y = \eta$) at $\partial\Omega_2$ and ($x = \xi - 0.08\sin(2\pi\xi)$, $y = 0$) at $\partial\Omega_3$. On the other hand, the grid system (c) was obtained by specifying the boundary correspondence on three sides as ($x = \xi$, $y = 0.8 + 0.2\cos(2\pi\xi)$) on $\partial\Omega_1$, ($x = 0$, $y = \eta$) on $\partial\Omega_2$, and ($x = \xi$, $y = 0$) at $\partial\Omega_3$. As we can see in the figure, the grid systems generated by Kang and Leal's method are coarse near the upper corners unless the boundary grid points at the bottom side are specified to be very dense near the lower corner points. However, in our new scheme, this problem can be avoided easily because the grid spacing near the upper corners can be controlled directly by specifying the boundary correspondence as we want. The orthogonality characteristics of the grid systems in Fig. 8 are shown in Table IV.

We tested also the adjustability of the grid spacing by the control parameter when the same boundary correspondence is specified. For the same region with the same boundary correspondence as in Fig. 8, the orthogonal grid systems were generated with the control function

$$q(v) = \frac{1}{2}\left[1 + \sin\left(\frac{v}{v^*}\pi - \frac{\pi}{2}\right)\right] + a\left[1 - \cos 2\left(\frac{v}{v^*}\right)\pi\right], \tag{26}$$

TABLE IV

Orthogonality Characteristics for the Grid Systems in Fig. 8

MDO–ADO (degrees)		
(a)	(b)	(c)
7.7–0.3	8.4–0.4	4.5–0.7

TABLE V

Orthogonality Characteristics for the Grid Systems in Fig. 9

MDO–ADO (degrees)			
(a)	(b)	(c)	(d)
3.9–0.6	6.4–1.2	3.1–0.7	5.0–0.8

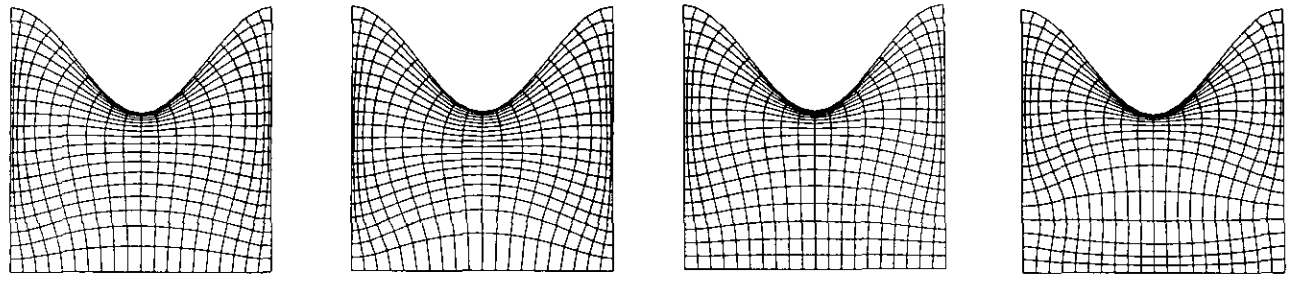

FIG. 9. The effect of parameter "a" in the control function $q(v) = \{1 + \sin((v/v^*)\pi - \pi/2)\}/2 + a\{1 - \cos 2(v/v^*)\pi\}$ on the orthogonal grid systems (the same geometry and boundary correspondence as in Fig. 8c): (a) $a = 0$; (b) $a = 0.1$; (c) $a = -0.1$; (d) $a = -0.2$.

where a is the control parameter mentioned earlier in Section 4. Several grid systems with various "a" are shown in Fig. 9. When $a = 0$ (Fig. 9a), the grid system is almost the same as that obtained with the control function $q(v) = 3(v/v^*)^2 - 2(v/v^*)^3$ (see Fig. 8c). When "a" is increased to the positive value ($a = 0.1$), the grid lines near $\xi = 0.5$ are attracted upward and the grid spacing near the $\eta = 0$ line ($\partial\Omega_3$) becomes too coarse (Fig. 9b)). On the other hand, when a negative value is used for "a" the grid lines are attracted downward. For example, when $a = -0.1$ (Fig. 9c), the resulting grid system has better grid distribution near the bottom line than the case $a = 0$ (Fig. 9a). However, when $a = -0.2$ (Fig. 9d), the central part of the grid becomes too coarse to be useful in numerical analysis. The orthogonality characteristics of the grid systems in Fig. 9 are generally good as shown in Table V. Especially, the grid system in Fig. 9c has excellent orthogonality characteristics in both MDO and ADO.

6. CONCLUSIONS

In the present paper, a new numerical scheme has been proposed for generating an orthogonal grid in an arbitrary simply-connected 2D domain. The scheme is based on the concept of the decomposition of the global orthogonal transform into consecutive mappings of a conformal mapping and an auxiliary orthogonal mapping, which was suggested by Kang and Leal [4].

The method is non-iterative and flexible in the adjustment of grid spacing. The grid spacing can be adjusted by specifying the boundary correspondence up to *three* sides of the boundary a priori. The method is also equipped with a control function that provides further degrees of freedom in grid spacing adjustment. The method has been applied very successfully to various geometries such as asymmetric wavy regions.

From a mathematical point of view, the proposed scheme can also be regarded as a numerical implementation of the *constructive* proof for the existence of a solution of the orthogonal mapping problem in an arbitrary simple-connected domain with the boundary correspondence specified on three sides a priori. However, the question of an existence proof for the problem of generating an orthogonal grid with specified boundary correspondence on all four sides still remains unanswered.

ACKNOWLEDGEMENT

This work was supported by a grant from the Korea Science and Engineering Foundation.

REFERENCES

1. J. F. Thompson, Z. U. A. Warsi, and C. W. Mastin, *Numerical Grid Generation* (North-Holland, New York, 1985).
2. B. Fornberg, *SIAM J. Sci. Stat. Comput.* **1**, 386 (1980).
3. G. T. Symm, *Numer. Math.* **9**, 250 (1966).
4. I. S. Kang and L. G. Leal, *J. Comput. Phys.* **102**, 78 (1992).
5. G. Ryskin and L. G. Leal, *J. Comput. Phys.* **50**, 71 (1983).
6. A. Allievi and S. M. Calisal, *J. Comput. Phys.* **98**, 163 (1992).
7. R. Duraiswami and A. Prosperetti, *J. Comput. Phys.* **98**, 254 (1992).
8. E. D. Chikliwala and Y. C. Yortsos, *J. Comput. Phys.* **57**, 391 (1985).
9. R. Menikoff and C. Zemach, *J. Comput. Phys.* **36**, 366 (1980).
10. H. J. Haussling and R. M. Coleman, *J. Comput. Phys.* **43**, 373 (1981).
11. K. Hsu and S. L. Lee, *J. Comput. Phys.* **96**, 451 (1991).